Journal of Molecular Spectroscopy **211,** 248–253 (2002)
doi:10.1006/jmsp.2001.8501, available online at http://www.idealibrary.com on IDEAL®

Intracavity Laser Spectroscopy of NiCl System G: Identification of a [13.0] $^2\Pi_{3/2}$ State

James J. O'Brien,*,[1] Joel S. Miller,*,[2] and L. C. O'Brien†

*Department of Chemistry, University of Missouri—St. Louis, St. Louis, Missouri 63121-4499; and †Department of Chemistry, Southern Illinois University Edwardsville, Edwardsville, Illinois 62026-1652

Received August 13, 2001; in revised form November 9, 2001

The (0,0) vibronic band of NiCl system G with a bandhead near 12 961 cm^{-1} was recorded at high resolution in absorption using intracavity laser spectroscopy (ILS). For the ILS absorption spectra, the NiCl molecules were produced in a nickel hollow cathode, operated with a small amount of CCl_4, and line positions were referenced to iodine spectra. Fourier transform (FT) emission spectroscopy was used to record an extensive region of the spectrum used in a vibronic analysis of system G. For the FT spectra, excited NiCl molecules were produced in a high-temperature King-type carbon tube furnace. We show that this transition is the (0,0) vibronic band associated with a newly identified $^2\Pi_{3/2}$ excited state and the $X^2\Pi_{3/2}$ ground state. The molecular constants for the new $^2\Pi_{3/2}$ electronic state are derived from the rotational analysis. Improved vibronic constants for the band are obtained from analysis of the FT spectra.

INTRODUCTION

The electronic structure of NiCl has received much attention recently, with various groups working on the pure rotational spectrum of the low-lying electronic states, the visible electronic transitions, and the near-infrared electronic transitions. The ground state electronic configuration of $Ni^+(3d^9)Cl^-(3p^6)$ gives rise to three low-lying electronic states: $X^2\Pi$, $A^2\Delta$, and $B^2\Sigma^+$ (e.g., see *1–3*). Excitation of one of the various nickel $3d$ electrons to an unoccupied nickel $4s$ or $4p$ orbital leads to numerous electronic transitions throughout the near-infrared and visible regions of the spectrum (*1–5*, and references contained in *6*).

In the microwave region, the pure rotational spectra of the $X^2\Pi_{3/2}$ states of all four major NiCl isotopomers were observed by Yamazaki *et al.* (*7*) in the region $J'' = 16.5$ to 37.5. Rotational transitions for the $A\,^2\Delta_{5/2}$ state also have been observed (*8*).

The Pinchemel and Bernath groups (*1–3*) have investigated the visible spectrum of NiCl via high-resolution laser-induced fluorescence and Fourier transform (FT) spectroscopy. They have established that NiCl has a $^2\Pi_{3/2}$ ground state, identified the other low-lying states (the $A^2\Delta_{5/2}$ state at 161.55 cm^{-1}, the $X^2\Pi_{1/2}$ state at 382 cm^{-1}, the $A^2\Delta_{3/2}$ state at 1646 cm^{-1}, and the $B^2\Sigma^+$ state at 1768 cm^{-1} and a state at 1385 cm^{-1}, the last possibly a quartet state) and identified several excited electronic states in the region 20 000–26 000 cm^{-1}. The pattern of low-lying states is in reasonable agreement with the known low-lying states of the isovalent molecule NiF (*9–13*).

The electronic transitions of NiCl occurring in the red and near-infrared region (6350–8750 Å) have been interpreted as consisting of many discrete band systems classified originally as system F through system J (*14*). Our previous work on NiCl system H (*4*) identified that transition as $^2\Sigma^+$–$X^2\Pi_{3/2}$, with the new $^2\Sigma^+$ state at 12,259 cm^{-1}. Additionally, we have shown that the NiCl system I is a transition between excited states (*5*) and does not connect to the low-lying $X^2\Pi$, $A^2\Delta$, or $B^2\Sigma^+$ state.

Little is known about NiCl system G. Rao *et al.* (*14*) published bandhead positions for the single-headed, red-degraded bands: the (0,0) band at 12 961.6 cm^{-1}, the (1,0) and (2,1) bands at 13 353.5 and 13 318.7 cm^{-1}, and the (2,0) and (3,1) bands at 13 742.3 and 13 701.2 cm^{-1}. They reported vibronic constants: $\nu_{0,0} = 12\,961.6$ cm^{-1}, $\omega'_e = 395.0$ cm^{-1}, $\omega_e x'_e = 1.55$ cm^{-1}, and $\omega_e = 424$ cm^{-1}.

We have used intracavity laser spectroscopy (ILS) techniques to record the near-infrared absorption spectrum of NiCl system G at rotational resolution and will show that system G is a transition between [13.0] $^2\Pi_{3/2}$, a newly identified electronic state, and the $X^2\Pi_{3/2}$ ground state. Improved vibronic constants are derived from FT spectra recorded for this band.

EXPERIMENTAL DETAILS

The spectrum of NiCl system G with a bandhead near 12 961 cm^{-1} was acquired in two ways. First, molecular emission from a carbon-type King furnace loaded with $NiCl_2$ was observed at medium resolution (0.04 cm^{-1}) using the Kitt Peak Fourier transform spectrometer. Approximately 25 g of anhydrous $NiCl_2$ was loaded into a King furnace and heated to 1500 C. A spectral region of 5000–20 000 cm^{-1} was recorded using

[1] Corresponding author. E-mail: obrien@jinx.umsl.edu.
[2] NSF STARS student scholar, Pattonville High School, St. Louis, Missouri.

0022-2852/02 $35.00

either a CaF_2 or a UV quartz beamsplitter and either InSb or silicon diode detectors. The high temperature (∼1500 C) and high pressures (300–500 Torr) employed in these experiments result in a measured linewidth of approximately 0.1 cm^{-1} FWHM. Many of the known visible and near-infrared NiCl systems were observed in the spectrum (*4–6*). This high-temperature spectrum was used in the vibronic analysis of NiCl system G. The second method of recording the NiCl system G spectrum entailed measurement of the molecular absorption spectrum at Doppler-limited resolution using the intracavity laser spectroscopy technique: an Ar plasma discharge is formed in a 2-inch-long nickel hollow cathode that is located in the resonator cavity of a Ti:sapphire laser, the NiCl species are created from sputtered nickel, and a tiny amount of CCl_4 mixed with the Ar flow through the cathode and the laser beam passes through the hollow cathode orifice. The spectrometer and method of data analysis are fully described in O'Brien *et al.* (*15, 16*) and Kalmar and O'Brien (*17*) and a description of the apparatus used to generate the gaseous NiCl is provided in O'Brien *et al.* (*4*).

The water-cooled hollow cathode used to produce NiCl is powered by an ENI DCG-100 DC plasma generator which is operated (250 to 500 V, up to 1.4 A) only for a short period of time initiated just before spectral data accumulation is started. Immediately following spectral acquisition with the plasma operating, a background spectrum is obtained using identical conditions except that the voltage is switched off and the current is 0.0 A. Division of the two dark-current-corrected spectra yields the spectrum of the plasma species.

Spectra are recorded as a series of overlapping, ∼6.4 cm^{-1} wide, spectral segments for the region 12 865–12 964 cm^{-1}. Calibration is accomplished by measuring alternatively the spectrum of the intracavity plasma species and an I_2 absorption spectrum (e.g., see Fig. 1) recorded from an extracavity cell. The ILS spectral output serves as the broadband spectral source for recording the I_2 spectrum which is obtained by dividing the spectrum obtained with I_2 present in the external cell with that obtained with I_2 absent from the cell. The widely used "Iodine Atlas" (*18*) is used as reference. To correct for small changes in the dispersion (∼1.6%) of the spectrum across the diode array, spectra recorded from a 14.7-mm-thick étalon provide a source of equally spaced fringes. Peak positions (absorption peaks and fringe positions) are determined from the zero crossing-points of the first derivative spectra using Savitzky–Golay polynomial smoothing. The procedure enables isolated, unblended line positions to be determined to an accuracy of better than ±0.002 cm^{-1}. Spectra were not deconvolved for the instrument function of the spectrograph. A typical linewidth of an isolated line is 0.037 cm^{-1} FWHM.

Whereas the FT spectra are hot and very congested, the ILS spectra are much less congested and this enables low-J transitions to be distinguished clearly; furthermore since the ILS spectra are viewed in real time, plasma conditions (voltage, current, pressure, mixing ratio) can be modified to enhance the selective formation of the measured lines.

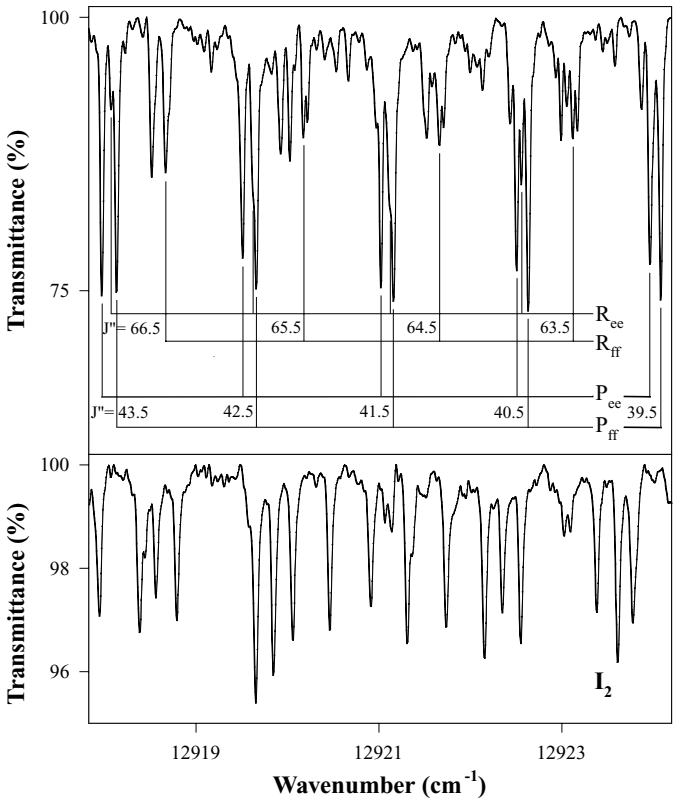

FIG. 1. A portion of the NiCl system G spectrum is presented in the upper panel. The corresponding iodine spectrum used for calibration is shown in the lower panel. Total pressure = 1.05 Torr. Assuming NiCl is observed only in the hollow cathode, the effective pathlength employed is 0.58 km.

RESULTS AND DISCUSSION

A vibronic analysis on system G was undertaken using the high-temperature FT spectrum recorded at Kitt Peak. Twelve vibronic bandheads associated with system G were observed and are listed in Table 1. The bandhead of each vibronic band was used to determine the vibrational constants for the electronic states of system G, and these are given in Table 2. The lower state vibrational frequency, $\omega_e = 426.7\ cm^{-1}$, indicated that the lower state of system G was quite possibly the $X^2\Pi_{3/2}$ state of NiCl (*1–3*).

TABLE 1
Observed Bandheads of System G, [13.0]
$^2\Pi_{3/2}$–$X^2\Pi_{3/2}$ (in cm^{-1})

v′ / v″	0	1	2	3	4
0	12961.5	13353.2	13742.0	14127.9	
1	12539.0	12931.7	13318.0	13705.5	14088.4
2	12119.1			13284.5	
3		12095.9			

TABLE 2
Vibrational Constants of NiCl System G, [13.0] $^2\Pi_{3/2}$–$X^2\Pi_{3/2}$ (in cm^{-1}, Using Bandheads)

	T_e	ω_e	$\omega_e x_e$
[13.0] $^2\Pi_{3/2}$	12978.0(12)	394.22(83)	1.38(18)
$X^2\Pi_{3/2}$	0.0	426.7(10)	1.85(30)

Note. One standard deviation is given in parenthesis.

TABLE 3
Molecular Constants for the (0,0) band of $^{58}Ni^{35}Cl$ System G, [13.0] $^2\Pi_{3/2}$–$X^2\Pi_{3/2}$ (in cm^{-1})

	$X\ ^2\Pi_{3/2}$	[13.0] $^2\Pi_{3/2}$
T_0	0.0	12959.2556(13)
B_0	0.181503836	0.1676970(20)
D_0	1.26770×10^{-7}	$1.2757(74) \times 10^{-7}$
H_0	-1.232×10^{-13}	$8.55(76) \times 10^{-13}$
q_J	1.15228×10^{-6}	$-8.135(71) \times 10^{-7}$
r_0	2.064 Å	2.147 Å

Note. One standard deviation is given in parenthesis. The ground state constants were held fixed to values from O'Brien *et al*. (*4*).

The (0,0) vibronic band of system G was observed with rotational resolution using the intracavity laser absorption technique. As shown in Fig. 2, the spectrum is degraded to the red with the R-bandhead occurring at relatively low J ($J \sim 10.5$). An R-branch and a P-branch were identified in the spectrum. Each branch splits into two branches at higher J, although the observed splitting was always small, <1.0 cm^{-1}, as shown in Figs. 1 and 2. These observations are consistent with an electronic transition of $^2\Pi_{3/2}$–$^2\Pi_{3/2}$ symmetry, where there are two strong R-branches, R_{ee} and R_{ff}, and two strong P-branches, P_{ee} and P_{ff}. The possible two Q-branches, Q_{ef} and Q_{fe}, are expected to be very weak and were not observed. Using the $X^2\Pi_{3/2}$ rotational constants obtained by O'Brien *et al*. (*4*) from our NiCl system H fit (which included the pure rotational transitions by Yamazaki *et al*. (*7*)), precise ground state levels were calculated. Definitive rotational assignments for the P_{ee} and R_{ee} branches and the P_{ff} and R_{ff} branches were obtained, using the fact that each pair of branches has a common upper state (*19*). Only lines due to the strongest NiCl isotopomer, $^{58}Ni^{35}Cl$, were clearly identified in the spectrum, although several spectra show additional structure, probably due to the other NiCl isotopomers, around the strong features in the spectra ($^{58}Ni^{35}Cl$ (51.58%), $^{60}Ni^{35}Cl$ (19.87%), $^{58}Ni^{37}Cl$ (16.50), and $^{60}Ni^{37}Cl$ (6.35%)).

A total of 247 lines from the [13.0] $^2\Pi_{3/2}$–$X^2\Pi_{3/2}$ transitions of the main NiCl isotopomer, $^{58}Ni^{35}Cl$, were fit using a nonlinear least squares fitting program. The upper and lower $^2\Pi_{3/2}$ energy levels were described by a polynomial expression previously used to fit $^2\Pi_{3/2}$ states in NiCl (*1, 4*). The molecular constants for the lower $X^2\Pi_{3/2}$ state were held fixed to the values from O'Brien *et al*. (*4*). The fit of the lines in the (0,0) vibronic band of system G of NiCl produced a set of five molecular constants for the newly identified [13.0] $^2\Pi_{3/2}$ state, and these are presented in Table 3. The average uncertainty of the individual rotational lines as determined from the standard deviation of the fit is 0.006 cm^{-1}. The observed rotational lines, assignments, and fit residuals are presented in Table 4.

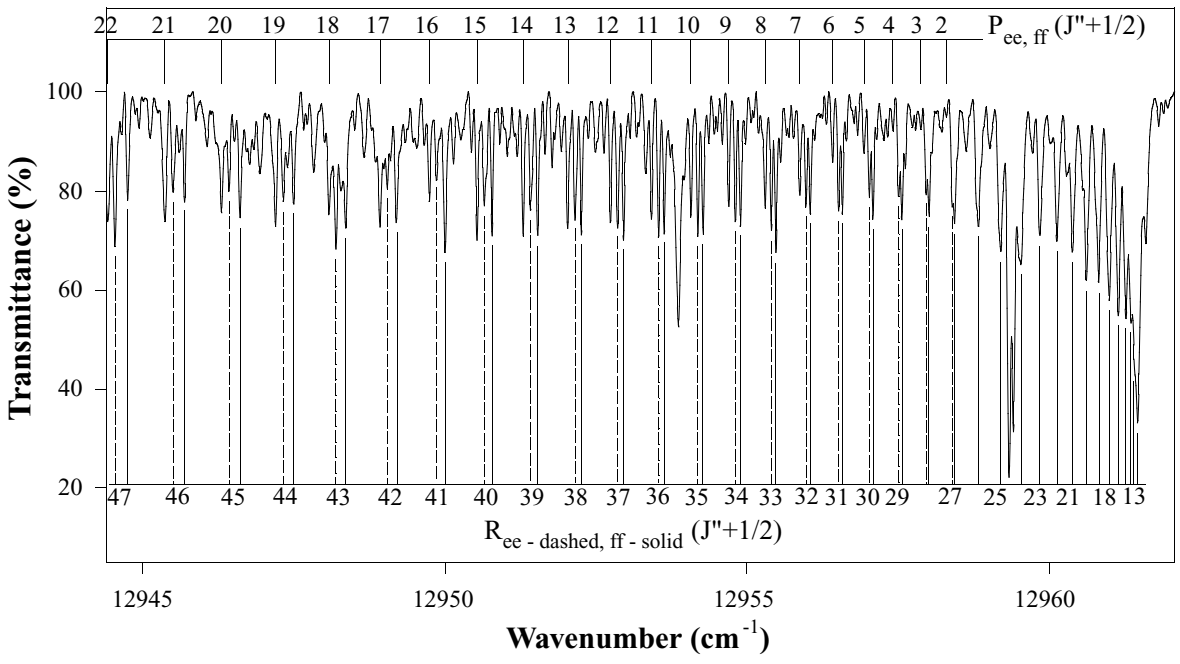

FIG. 2. The bandhead region of the (0,0) band of NiCl system G. The P_{ee}, P_{ff} splitting is not distinguishable at the lower J values.

TABLE 4
Line Positions, Assignments, and Residuals for $^{58}Ni^{35}Cl$ System G, [13.0] $^2\Pi_{3/2}$–$X^2\Pi_{3/2}$ (in cm^{-1})

J''	$P_{ee}(J'')$	o - c	$P_{ff}(J'')$	o - c	$R_{ee}(J'')$	o - c	$R_{ff}(J'')$	o - c
3.5	12957.860	−0.005	12957.860	−0.005				
4.5	12957.420	0.015	12957.420	0.015				
5.5	12956.923	0.005	12956.923	0.005				
6.5	12956.401	−0.002	12956.401	−0.002				
7.5	12955.859	−0.001	12955.859	−0.002				
8.5	12955.284	−0.006	12955.284	−0.007				
9.5	12954.684	−0.008	12954.684	−0.010				
10.5	12954.058	−0.009	12954.058	−0.011				
11.5	12953.410	−0.003	12953.410	−0.006				
12.5	12952.732	−0.001	12952.732	−0.004	12961.455	0.005	12961.455	0.000
13.5	12952.024	0.000	12952.024	−0.005	12961.424	0.012	12961.424	0.006
14.5	12951.289	0.001	12951.289	−0.005	12961.348	0.002	12961.348	−0.005
15.5	12950.540	0.016	12950.540	0.008	12961.266	0.014	12961.267	0.006
16.5	12949.747	0.014	12949.747	0.005	12961.139	0.009	12961.140	−0.001
17.5	12948.931	0.017	12948.931	0.007	12960.984	0.003	12960.979	−0.014
18.5	12948.084	0.017	12948.084	0.005	12960.812	0.008	12960.812	−0.006
19.5	12947.216	0.023	12947.216	0.009	12960.610	0.011	12960.607	−0.009
20.5	*12946.315	0.025	*12946.315	0.008	*12960.381	0.015	*12960.381	−0.005
21.5	*12945.383	0.022	*12945.383	0.003	*12960.122	0.016	*12960.121	−0.007
22.5	*12944.409	0.006	*12944.409	−0.017	*12959.841	0.023	*12959.842	−0.001
23.5	*12943.436	0.018	*12943.436	−0.008	*12959.522	0.020	*12959.530	0.000
24.5	*12942.417	0.012	*12942.417	−0.017	12959.175	0.017	12959.186	−0.004
25.5	*12941.384	0.019	*12941.384	−0.014	12958.793	0.007	12958.810	−0.012
26.5	*12940.314	0.017	*12940.335	0.002	12958.389	0.003	12958.417	−0.009
27.5	12939.210	0.009	12939.241	−0.001	12957.956	−0.003	12957.986	−0.018
28.5	12938.086	0.009	12938.117	−0.006	12957.500	−0.004	12957.549	−0.004
29.5	12936.931	0.005	12936.981	0.004	12957.018	−0.002	12957.071	−0.004
30.5	12935.748	0.001	12935.801	−0.002	12956.503	−0.006	12956.558	−0.012
31.5	12934.545	0.004	12934.600	−0.002	12955.964	−0.007	12956.035	−0.002
32.5	12933.307	0.000	12933.373	−0.001	12955.390	−0.014	12955.466	−0.010
33.5	12932.045	0.000	12932.118	−0.001	12954.794	−0.015	12954.877	−0.011
34.5	12930.751	−0.004	12930.841	0.005	12954.175	−0.012	12954.260	−0.013
35.5	12929.432	−0.006	12929.530	0.004	12953.527	−0.009	12953.621	−0.009
36.5	12928.089	−0.004	12928.204	0.016	12952.851	−0.007	12952.948	−0.012
37.5	12926.719	−0.001	12926.833	0.009	12952.149	−0.003	12952.252	−0.010
38.5	12925.318	−0.002	12925.436	0.004	12951.415	−0.003	12951.527	−0.010
39.5	12923.897	0.005	12924.006	−0.007	12950.673	0.017	12950.772	−0.012
40.5	12922.439	0.002	12922.562	−0.005	12949.880	0.014	12950.018	0.014
41.5	12920.953	0.000	12921.086	−0.007	12949.060	0.012	12949.212	0.015
42.5	12919.439	−0.004	12919.585	−0.008	12948.212	0.010	12948.374	0.012
43.5	12917.903	−0.001	12918.063	−0.002	12947.339	0.010	12947.512	0.013
44.5	12916.338	0.000	12916.511	0.001	12946.439	0.012	12946.623	0.013
45.5	12914.746	0.002	12914.933	0.005	12945.488	−0.010	12945.703	0.011
46.5	12913.122	0.000	12913.324	0.005	12944.524	−0.017	12944.761	0.013
47.5	12911.474	0.001	12911.681	−0.002	12943.540	−0.016	12943.763	−0.013
48.5	12909.803	0.006	12910.021	0.001	12942.536	−0.006	12942.763	−0.014
49.5	12908.100	0.008	12908.329	−0.001	12941.496	−0.005	12941.748	−0.003
50.5	12906.367	0.007	12906.615	0.003	12940.431	−0.002	12940.685	−0.012
51.5	12904.603	0.002	12904.873	0.005	12939.326	−0.010	12939.617	0.001
52.5	12902.814	0.000	12903.098	0.001	12938.209	−0.002	12938.507	−0.001
53.5	12900.999	0.000	12901.301	0.002	12937.053	−0.006	12937.370	−0.002
54.5	12899.158	0.001	12899.475	0.002	12935.879	0.000	12936.215	0.005
55.5	12897.290	0.003	12897.623	0.002	12934.675	0.005	12935.025	0.005
56.5	12895.396	0.006	12895.741	−0.002	12933.434	0.000	12933.805	0.002
57.5	12893.467	0.002	12893.834	−0.003	12932.566	0.008	12932.566	0.008
58.5	12891.510	−0.003	12891.903	−0.001	12931.291	0.004	12931.291	0.004
59.5					12929.555	0.000	12929.995	0.006
60.5					12928.200	−0.008	12928.668	0.005
61.5					12926.833	0.000	12927.316	0.005

*Blended lines, deweighted slightly in fit.

TABLE 4—*Continued*

J''	$P_{ee}(J'')$	o - c	$P_{ff}(J'')$	o - c	$R_{ee}(J'')$	o - c	$R_{ff}(J'')$	o - c
62.5					12925.436	0.006	12925.938	0.007
63.5					12924.009	0.010	12924.520	−0.004
64.5					12922.541	0.000	12923.098	0.007
65.5					12921.043	−0.012	12921.634	0.003
66.5					12919.549	0.008	12920.149	0.006
67.5					12918.005	0.006	12918.629	0.000
68.5					12916.427	−0.003	12917.084	−0.004
69.5					12914.827	−0.007	12915.518	−0.002
70.5					12913.207	−0.002	12913.922	−0.004
71.5					12911.557	−0.001	12912.305	0.000
72.5					12909.872	−0.007	12910.661	0.004
73.5					12908.179	0.007	12908.979	−0.004
74.5					12906.418	−0.020	12907.278	−0.004
75.5					12904.658	−0.019	12905.545	−0.010
76.5							12903.794	−0.007
77.5							12902.016	−0.005
78.5							12900.213	−0.001
79.5							12898.375	−0.006
80.5							12896.510	−0.012
81.5							12894.632	−0.005
82.5							12892.729	0.003
83.5							12890.802	0.013
84.5							12888.838	0.012

From the B_0 rotational constants, the bond length of the NiCl molecule can be determined for each state: $r_0(X^2\Pi_{3/2}) = 2.064$ Å and $r_0([13.0]^2\Pi_{3/2}) = 2.147$ Å. An increase in the bond length is noted, >0.08 Å. The bond length in the $[13.0]^2\Pi_{3/2}$ state also is larger than the value determined for the nearby $[12.3]^2\Sigma^+$ state which we recently observed (*4*): $r_0([12.3]^2\Sigma^+) = 2.130$ Å. The ground state and low-lying electronic states (T_0's < 2000 cm^{-1}) are consistent with the electron configuration $Ni^+(3d^9)Cl^-(3p^{10})$ (*1–3*). Since the valence electrons are metal-centered, we expect the excited electronic states with term energies in the region 4000–25 000 cm^{-1} to correlate to excited state Ni^+ orbitals, for example, such as the $Ni^+(3d^84s^1)Cl^-(3d^{10})$ electron configuration (*20*). Thus the increase in bond length is not attributable to charge-transfer excitation in NiCl. A high-level *ab initio* calculation of the excited states of NiCl would be of great benefit in giving insight as to the nature of the new $[12.3]^2\Sigma^+$ and $[13.0]^2\Pi_{3/2}$ state.

Since the $Cl^-(3d^{10})$ ligand is not directly participating in covalent bonding and the electronic excitation is metal-centered, we predict that the NiCl, NiBr, and NiI molecules will display very similar electronic spectra. We believe our $[13.0]^2\Pi_{3/2}$–$X^2\Pi_{3/2}$ transition of NiCl is analogous to the $[12.7]^2\Pi_{3/2}$–$X^2\Pi_{3/2}$ transition of NiBr which was observed recently at high resolution by Cheung and co-workers (*21*).

CONCLUSIONS

The (0,0) band of NiCl system G was observed by intracavity laser absorption spectroscopy. The rotational analysis of this system has shown that it is the $[13.0]^2\Pi_{3/2}$–$X^2\Pi_{3/2}$ transition, where the $[13.0]^2\Pi_{3/2}$ state has been identified for the first time. Molecular parameters for the new electronic state are provided.

ACKNOWLEDGMENTS

Partial support for this work was provided by the Petroleum Research Fund (LCO'B). The Ti:sapphire laser employed was funded by an equipment grant from NASA's Planetary Atmospheres program (JJO'B).

REFERENCES

1. T. Hirao, C. Dufour, B. Pinchemel, and P. F. Bernath, *J. Mol. Spectrosc.* **202,** 53–58 (2000).
2. A. Poclet, Y. Krouti, T. Hirao, B. Pinchemel, and P. F. Bernath, *J. Mol. Spectrosc.* **204,** 125–132 (2000).
3. Y. Krouti, A. Poclet, T. Hirao, B. Pinchemel, and P. F. Bernath, *J. Mol. Spectrosc.* **210,** 41–50 (2001).
4. L. C. O'Brien, K. M. Homann, T. L. Kellerman, and J. J. O'Brien, *J. Mol. Spectrosc.* **211,** 93–98 (2002).
5. L. C. O'Brien, T. L. Kellerman, and J. J. O'Brien, submitted for publication.
6. K. Huber and G. Herzberg, "Constants of Diatomic Molecules," Van Nostrand–Reinhold, New York, 1975.
7. E. Yamazaki, T. Okabayashi, and M. Tanimoto, *Astrophys. J.* **551,** L199–L201 (2001).
8. M. Tanimoto, personal communication.
9. C. Dufour, P. Carette, and B. Pinchemel, *J. Mol. Spectrosc.* **148,** 303–309 (1991).
10. C. Dufour, I. Hikmet, and B. Pinchemel, *J. Mol. Spectrosc.* **165,** 398–405 (1994).
11. C. Dufour and B. Pinchemel, *J. Mol. Spectrosc.* **173,** 70–78 (1995).

12. C. Focsa, C. Dufour, and B. Pinchemel, *J. Mol. Spectrosc.* **182,** 65–71 (1997).
13. Y. Chen, J. Jin, C. Hu, X. Yang, X. Ma, and C. Chen, *J. Mol. Spectrosc.* **203,** 37–40 (2000).
14. S. V. K. Rao, S. P. Reddy, and P. T. Rao, *Z. Phys.* **166,** 261–264 (1962).
15. L. C. O'Brien, H. Cao, and J. J. O'Brien, *J. Mol. Spectrosc.* **199,** 100–108 (2000).
16. L. C. O'Brien, H. Cao, and J. J. O'Brien, *J. Mol. Spectrosc.* **207,** 99–103 (2001).
17. B. Kalmar and J. J. O'Brien, *J. Mol. Spectrosc.* **192,** 386–393 (1998).
18. S. Gerstenkorn, J. Verges, and J. Chevillard, "Atlas du Spectre d'Absorption de la Molecule d'Iode. Vol. III. 11,000–14,000 cm^{-1}," Laboratoire Aimé Cotton, CNRS II, Orsay, 1982.
19. G. Herzberg, "Spectra of Diatomic Molecules," Van Nostrand Reinhold, 1950.
20. C. E. Moore, "Atomic Energy Levels," NSRDS-NBS **35,** 1975.
21. A. S.-C. Cheung, J. W.-H. Leung, J. Dai, and X. Wang, "Laser Spectroscopy of NiBr: Rotational Analysis of the $^2\Pi_{3/2}$–$X\,^2\Pi_{3/2}$ transition," Paper FC04, *presented at the 56th Ohio State University International Symposium on Molecular Spectroscopy*, Columbus, Ohio, June 11–15, 2001.